Appearance-Disappearance Relation in 3+N_s Short-Baseline Neutrino Oscillations

C. Giunti[1] and E. M. Zavanin[1,2,3]
[1] *INFN, Sezione di Torino, Via P. Giuria 1, I–10125 Torino, Italy*
[2] *Department of Physics, University of Torino, Via P. Giuria 1, I–10125 Torino, Italy*
[3] *Instituto de Física Gleb Wataghin, Universidade Estadual de Campinas - UNICAMP, Rua Sérgio Buarque de Holanda, 777, 13083-859 Campinas SP Brazil*
(Dated: 14 September 2015)

We derive the relation between the amplitudes of short-baseline appearance and disappearance oscillations in 3+N_s neutrino mixing schemes which is the origin of the appearance-disappearance tension that is found from the analysis of the existing data in any 3+N_s neutrino mixing scheme. We illustrate the power of the relation to reveal the appearance-disappearance tension in the cases of 3+1 and 3+2 mixing using the results of global fits of short-baseline neutrino oscillation data.

PACS numbers: 14.60.Pq, 14.60.St

The standard three-neutrino mixing scheme, which explains the oscillations that have been observed in solar, reactor and accelerator experiments (see [1, 2]), may be an incomplete description of neutrino mixing, as suggested by the indications in favor of short-baseline oscillations generated by a squared-mass difference $\Delta m^2_{\text{SBL}} \sim 1\,\text{eV}^2$ which is much larger than the standard "solar" ($\Delta m^2_{\text{SOL}} \approx 7.5\times10^{-5}\,\text{eV}^2$) and "atmospheric" ($\Delta m^2_{\text{ATM}} \approx 2.4\times10^{-3}\,\text{eV}^2$) squared-mass differences characteristic of three-neutrino mixing.

The indications in favor of short-baseline oscillations are: the reactor antineutrino anomaly [3], which is a deficit of the rate of $\bar{\nu}_e$ observed in several short-baseline reactor neutrino experiments in comparison with that expected from the latest calculation of the reactor neutrino fluxes [4, 5]; the Gallium neutrino anomaly [6–10], consisting in a short-baseline disappearance of ν_e measured in the Gallium radioactive source experiments GALLEX [11] and SAGE [12]; the signal of short-baseline $\bar{\nu}_\mu \to \bar{\nu}_e$ oscillations observed in the LSND experiment [13, 14].

These results can be explained by extending the standard framework of three-neutrino mixing with the introduction of new massive neutrinos that in the flavor basis correspond to sterile neutrinos [15], which do not have standard weak interactions. The simplest scheme is that called "3+1", in which there are the three standard active neutrinos ν_e, ν_μ, ν_τ, and one new sterile neutrino ν_s. In the mass basis, there are the three standard massive neutrinos ν_1, ν_2, ν_3, whose two independent squared-mass differences correspond to Δm^2_{SOL} and Δm^2_{ATM}, and an additional massive neutrino ν_4 which generates the short-baseline squared-mass difference $\Delta m^2_{41} \simeq \Delta m^2_{42} \simeq \Delta m^2_{43} \simeq \Delta m^2_{\text{SBL}}$ (with the usual definition $\Delta m^2_{jk} = m^2_j - m^2_k$, where m_k is the mass of ν_k).

However, it is possible that there are more than one new massive neutrinos which generate more than one $\Delta m^2_{\text{SBL}} \gtrsim 1\,\text{eV}^2$. In the literature one can find studies of 3+2 [16–20], 3+3 [18], 3+1+1 [21–24], and 1+3+1 [25, 26] schemes. It turns out that in all these schemes there is a tension between the results of short-baseline appearance and disappearance experiments [16, 18–20, 25–44]. The reason of this tension is well understood in the framework of the 3+1 mixing scheme from the analytic relation which connects the amplitudes of appearance and disappearance short-baseline oscillations [27, 28]. In this paper we extend this explanation to the general case of 3+N_s mixing, in which there are N_s mostly sterile massive neutrinos at the eV scale (some of which can also be at a larger scale).

For the study of neutrino oscillations in vacuum it is convenient to use the following general expression of the probability of $\overset{(-)}{\nu}_\alpha \to \overset{(-)}{\nu}_\beta$ oscillations [45, 46]:

$$P_{\substack{(-)\\ \nu_\alpha\to\nu_\beta}}^{\substack{(-)}} = \delta_{\alpha\beta} - 4\sum_{k\neq p} |U_{\alpha k}|^2 \left(\delta_{\alpha\beta} - |U_{\beta k}|^2\right) \sin^2\Delta_{kp} + 8\sum_{\substack{j>k\\ j,k\neq p}} |U_{\alpha j}U_{\beta j}U_{\alpha k}U_{\beta k}| \sin\Delta_{kp}\sin\Delta_{jp} \times \cos(\Delta_{jk} \overset{(+)}{-} \eta_{\alpha\beta jk}), \qquad (1)$$

where

$$\Delta_{kp} = \frac{\Delta m^2_{kp} L}{4E}, \qquad \eta_{\alpha\beta jk} = \arg\left[U^*_{\alpha j} U_{\beta j} U_{\alpha k} U^*_{\beta k}\right], \quad (2)$$

and p is an arbitrary fixed index, which can be chosen in the most convenient way depending on the case under consideration. In the case of three-neutrino mixing, there is only one interference term in Eq. (1), because for any choice of p there is only one possibility for j and k such that $j > k$.

In the following we take into account that the non-standard massive neutrinos must be mostly sterile, i.e.

$$|U_{\alpha k}|^2 \ll 1 \qquad (\alpha = e,\mu,\tau; \quad k = 4,\ldots,N), \quad (3)$$

in order not to spoil the successful three-neutrino mixing explanation of solar, atmospheric and long-baseline neutrino oscillation measurements. The non-standard massive neutrinos are conveniently labeled in order of increasing mass: $m_4 \leq m_5 \leq \ldots \leq m_N$.

We are interested in the effective oscillation probabilities in short-baseline experiments, for which $\Delta_{21} \ll$

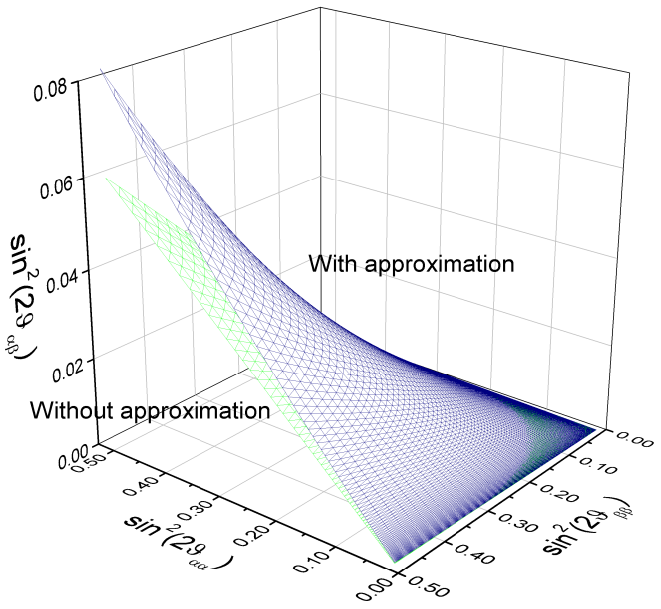

FIG. 1. Three-dimensional illustration of the relation in Eq. (9) (without approximation) and the approximated relation in Eq. (10) (with approximation).

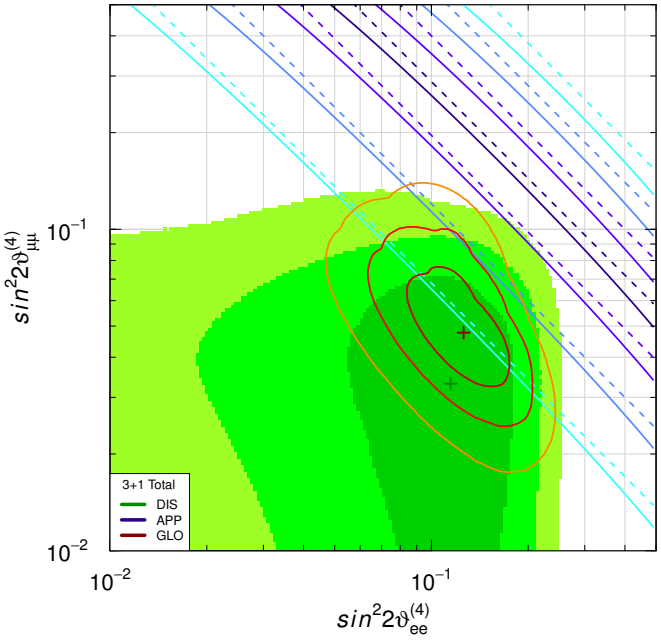

FIG. 2. Allowed regions in the $\sin^2 2\vartheta^{(4)}_{ee}$–$\sin^2 2\vartheta^{(4)}_{\mu\mu}$ plane obtained in the total 3+1 fit of short-baseline data corresponding to the 3+1-LOW fit of Ref. [44]. The green shadowed regions are the regions allowed at 1σ, 2σ and 3σ by the analysis of short-baseline disappearance (DIS) data, with the best fit value indicated by a dark-green cross. The strips enclosed by the blue diagonal lines are allowed at 1σ, 2σ and 3σ by the analysis of short-baseline appearance (APP) data, with the central best fit dark-blue line. The solid lines correspond to the exact relation in Eq. (9), whereas the dashed lines correspond to the approximated relation in Eq. (10). The regions inside the red-orange closed curves are allowed at 1σ, 2σ and 3σ by the global (GLO) analysis of short-baseline data, with the best fit value indicated by a dark-red cross.

$\Delta_{31} \ll 1$. In the general case of $3{+}N_s$ mixing with $\Delta m^2_{k1} \gtrsim \Delta m^2_{\rm SBL}$ and $\Delta_{k1} \gtrsim 1$ for $k \geq 4$, choosing $p = 1$ in Eq. (2) we obtain

$$P^{\rm (SBL)}_{\substack{(-)\\ \nu_\alpha \to \nu_\beta}} \simeq \delta_{\alpha\beta} - 4 \sum_{k=4}^{N} |U_{\alpha k}|^2 \left(\delta_{\alpha\beta} - |U_{\beta k}|^2\right) \sin^2 \Delta_{k1} + 8 \sum_{k=4}^{N} \sum_{j=k+1}^{N} |U_{\alpha j} U_{\beta j} U_{\alpha k} U_{\beta k}| \sin \Delta_{k1} \sin \Delta_{j1} \times \cos(\Delta_{jk} \overset{(+)}{-} \eta_{\alpha\beta jk}). \quad (4)$$

Considering the survival probabilities of active neutrinos, let us define the effective amplitudes

$$\sin^2 2\vartheta^{(k)}_{\alpha\alpha} = 4|U_{\alpha k}|^2 \left(1 - |U_{\alpha k}|^2\right) \simeq 4|U_{\alpha k}|^2, \quad (5)$$

for $\alpha = e, \mu, \tau$ and $k \geq 4$. The approximation is due to the constraint (3), which allows to neglect the quadratically suppressed contribution proportional to $|U_{\alpha k}|^4$. Dropping the quadratically suppressed terms also in the survival probabilities, we obtain

$$P^{\rm (SBL)}_{\substack{(-)\\ \nu_\alpha \to \nu_\alpha}} \simeq 1 - \sum_{k=4}^{N} \sin^2 2\vartheta^{(k)}_{\alpha\alpha} \sin^2 \Delta_{k1}, \quad (6)$$

for $\alpha = e, \mu, \tau$. Hence, each effective mixing angle $\vartheta^{(k)}_{\alpha\alpha}$ parameterizes the disappearance of $\overset{(-)}{\nu}_\alpha$ due to its mixing with $\overset{(-)}{\nu}_k$ for $k \geq 4$.

Let us now consider the probabilities of short-baseline $\overset{(-)}{\nu}_\alpha \to \overset{(-)}{\nu}_\beta$ transitions between two different active neutrinos or an active and a sterile neutrino. We define the transition amplitudes

$$\sin^2 2\vartheta^{(k)}_{\alpha\beta} = 4|U_{\alpha k}|^2 |U_{\beta k}|^2, \quad (7)$$

for $\alpha \neq \beta$ and $k \geq 4$, which allow us to write the transition probabilities as

$$P^{\rm (SBL)}_{\substack{(-)\\ \nu_\alpha \to \nu_\beta}} \simeq \sum_{k=4}^{N} \sin^2 2\vartheta^{(k)}_{\alpha\beta} \sin^2 \Delta_{k1} + 2 \sum_{k=4}^{N} \sum_{j=k+1}^{N} \sin 2\vartheta^{(k)}_{\alpha\beta} \sin 2\vartheta^{(j)}_{\alpha\beta} \sin \Delta_{k1} \sin \Delta_{j1} \times \cos(\Delta_{jk} \overset{(+)}{-} \eta_{\alpha\beta jk}). \quad (8)$$

From the first line one can see that each effective mixing angle $\vartheta^{(k)}_{\alpha\beta}$ parameterizes the amount of $\overset{(-)}{\nu}_\alpha \to \overset{(-)}{\nu}_\beta$ transitions due to the mixing of $\overset{(-)}{\nu}_\alpha$ and $\overset{(-)}{\nu}_\beta$ with $\overset{(-)}{\nu}_k$ for $k \geq 4$. The second line in Eq. (8) is the interference between the $\overset{(-)}{\nu}_k$ and $\overset{(-)}{\nu}_j$ contributions for $k, j \geq 4$, which depends on the same effective mixing angles.

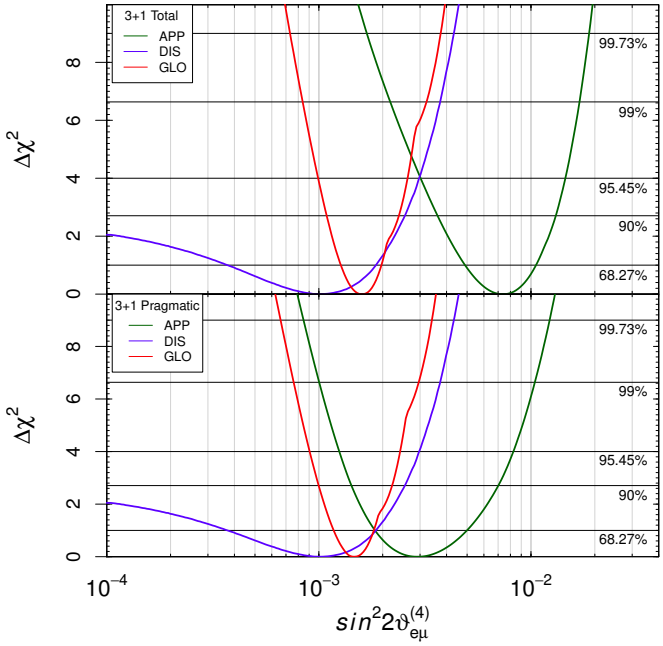

FIG. 3. Marginal $\Delta\chi^2$ as a function of $\sin^2 2\vartheta^{(4)}_{e\mu}$ obtained in the total (upper panel) and pragmatic (lower panel) 3+1 analyses of short-baseline data presented in Ref. [44]. The horizontal lines gives the values of $\Delta\chi^2$ corresponding to 68.27% C.L. (1σ), 90% C.L., 95.45% C.L. (2σ), 99% C.L. and 99.73% C.L. (3σ) for one degree of freedom. The curves obtained from disappearance (DIS) data are equal in the two panels.

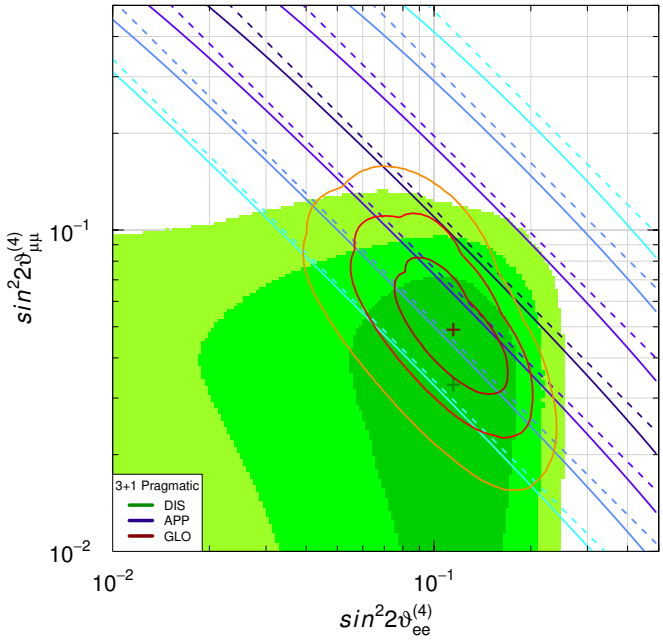

FIG. 4. Allowed regions in the $\sin^2 2\vartheta^{(4)}_{ee}$–$\sin^2 2\vartheta^{(4)}_{\mu\mu}$ plane obtained in the pragmatic 3+1 fit of short-baseline data corresponding to the 3+1-HIG fit of Ref. [44]. See the caption of Fig. 2. The green shadowed regions obtained from disappearance (DIS) data are the same of Fig. 2.

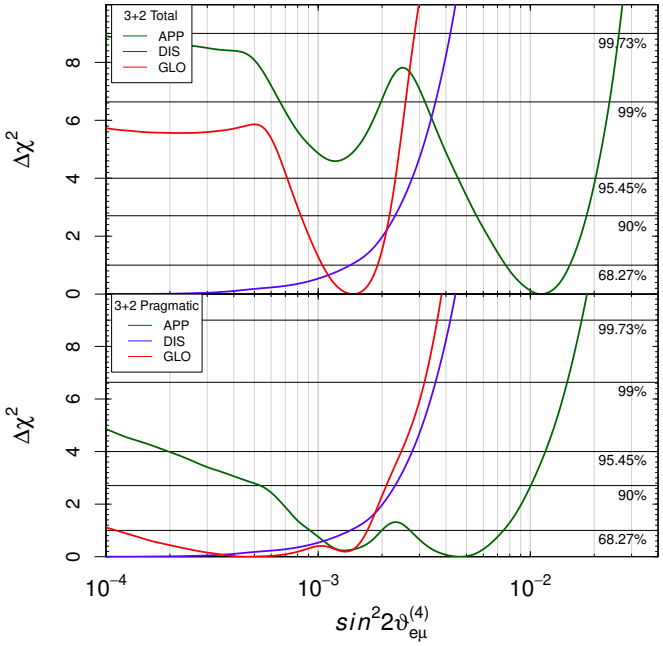

FIG. 5. Marginal $\Delta\chi^2$ as a function of $\sin^2 2\vartheta^{(4)}_{e\mu}$ obtained in the total (upper panel) and pragmatic (lower panel) 3+2 fits of short-baseline data presented in Ref. [44]. See the caption of Fig. 3.

Considering now the transitions between two different active neutrinos, from Eqs. (5) and (7) one can see that for each value of $k \geq 4$ the transition amplitude $\sin 2\vartheta^{(k)}_{\alpha\beta}$ and the disappearance amplitudes $\sin 2\vartheta^{(k)}_{\alpha\alpha}$ and $\sin 2\vartheta^{(k)}_{\beta\beta}$ depend only on the elements in $k^{\rm th}$ column of the mixing matrix and are related by

$$\sin^2 2\vartheta^{(k)}_{\alpha\beta} = \left(1 - \sqrt{1 - \sin^2 2\vartheta^{(k)}_{\alpha\alpha}}\right) \times \left(1 - \sqrt{1 - \sin^2 2\vartheta^{(k)}_{\beta\beta}}\right), \qquad (9)$$

for $\alpha = e, \mu, \tau$. Taking into account the constraint (3), we have

$$\sin^2 2\vartheta^{(k)}_{\alpha\beta} \simeq \frac{1}{4} \sin^2 2\vartheta^{(k)}_{\alpha\alpha} \sin^2 2\vartheta^{(k)}_{\beta\beta}, \qquad (10)$$

as illustrated in Fig. 1. This relation was derived in the case of 3+1 mixing and $k = 4$ in Refs. [27, 28]. Now we see that the same relation is valid in the general case of $3+N_s$ mixing between the amplitudes of appearance and disappearance oscillations due to each squared-mass difference Δm^2_{k1} generated by a non-standard mostly sterile massive neutrino at the eV scale (or at a larger scale). Note that the relation is very powerful in the global fit of short-baseline oscillation data, because it constrain the appearance and disappearance amplitudes for any fixed value of the corresponding squared-mass difference.

The relation (9) is very important, because it constraints the oscillation signals that can be observed

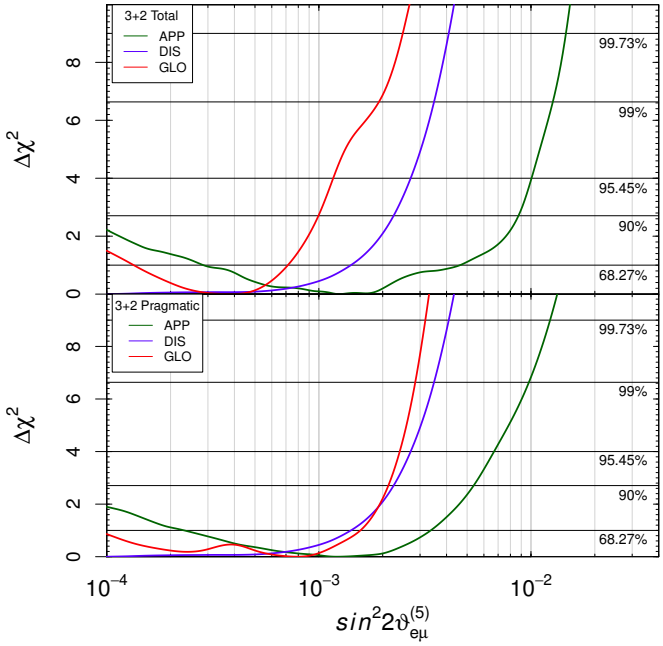

FIG. 6. Marginal $\Delta\chi^2$ as a function of $\sin^2 2\vartheta^{(5)}_{e\mu}$ obtained in the total (upper panel) and pragmatic (lower panel) 3+2 fits of short-baseline data presented in Ref. [44]. See the caption of Fig. 3.

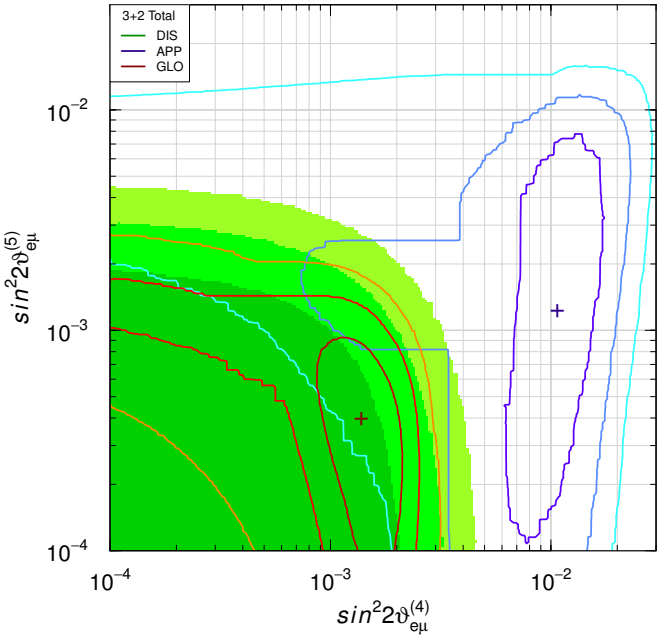

FIG. 7. Allowed regions in the $\sin^2 2\vartheta^{(4)}_{e\mu}$–$\sin^2 2\vartheta^{(5)}_{e\mu}$ plane obtained in the total 3+2 fit of short-baseline data corresponding to the 3+2-LOW fit of Ref. [44]. The green shadowed regions are the regions allowed at 1σ, 2σ and 3σ by the analysis of short-baseline disappearance (DIS) data, with the best fit value at $\sin^2 2\vartheta^{(4)}_{e\mu} = \sin^2 2\vartheta^{(5)}_{e\mu} = 0$. The regions inside the blue closed curves are allowed at 1σ, 2σ and 3σ by the analysis of short-baseline appearance (APP) data, with the best fit value indicated by a dark-blue cross. The regions inside the red-orange closed curves are allowed at 1σ, 2σ and 3σ by the global (GLO) analysis of short-baseline data, with the best fit value indicated by a dark-red cross.

in short-baseline appearance and disappearance experiments in any $3{+}N_s$ mixing scheme with sterile neutrinos. Its experimental test is crucial for the acceptance or rejection of these schemes. In particular, since both $\sin^2 2\vartheta^{(k)}_{ee}$ and $\sin^2 2\vartheta^{(k)}_{\mu\mu}$ are small, the amplitudes of short-baseline $\overset{(-)}{\nu}_\mu \leftrightarrows \overset{(-)}{\nu}_e$ transitions implied by the results of disappearance experiments are quadratically suppressed and in tension with the short-baseline $\bar{\nu}_\mu \to \bar{\nu}_e$ transitions observed in the LSND experiment [16, 18–20, 25–44].

In the following we illustrate the importance of the constraint (9) (and its approximation (10)) in the cases of 3+1 and 3+2 mixing using the results of the fits of short-baseline neutrino oscillation data presented in Ref. [44]. We denote with the labels "APP" and "DIS" the fits of appearance and disappearance data alone, respectively. The label "GLO" denotes the global combined fit of appearance and disappearance data. Furthermore, we distinguish between "total" and "pragmatic" fits. A total fit corresponds to a "LOW" fit in Ref. [44], in which all the data of short-baseline neutrino oscillation experiments considered in Ref. [44] are taken into account. A pragmatic fit corresponds to a "HIG" fit in Ref. [44], in which all the data of short-baseline neutrino oscillation experiments considered in Ref. [44] are taken into account except the anomalous low-energy bins of the MiniBooNE experiment [47, 48]. This "pragmatic approach" was advocated in Ref. [44] because the anomalous low-energy bins of the MiniBooNE experiment [47, 48] are incompatible with neutrino oscillations and may be due to background (this problem is going to be investigated in the MicroBooNE experiment [49, 50]). Note that only the APP and GLO fits are different in the total and a pragmatic fits, whereas the DIS fit of disappearance data is the same.

Figure 2 shows the regions in the $\sin^2 2\vartheta^{(4)}_{ee}$–$\sin^2 2\vartheta^{(4)}_{\mu\mu}$ plane allowed at 1σ, 2σ and 3σ by the total 3+1 fit of short-baseline data presented in Ref. [44] (corresponding to the "3+1-LOW" fit in Ref. [44]). One can see that there is a clear tension between the regions allowed by disappearance and appearance data. The relation (9) allows us to illustrate the tension also by showing the marginal $\Delta\chi^2$ as a function of $\sin^2 2\vartheta^{(4)}_{e\mu}$ in the upper panel of Fig. 3. One can see that there is no overlap of the intervals of $\sin^2 2\vartheta^{(4)}_{e\mu}$ allowed by the appearance and disappearance data at less than about 2σ and the result of the global fit is a compromise with the best-fit dominated by the disappearance data.

The fit of the anomalous MiniBooNE low-energy bins with 3+1 neutrino oscillations requires a small value of Δm^2_{41} and a large value of $\sin^2 2\vartheta^{(4)}_{e\mu}$, which are in strong tension with the data of disappearance experiments [39, 40, 44]. Hence, we can alleviate the appearance-disappearance tension by adopting the prag-

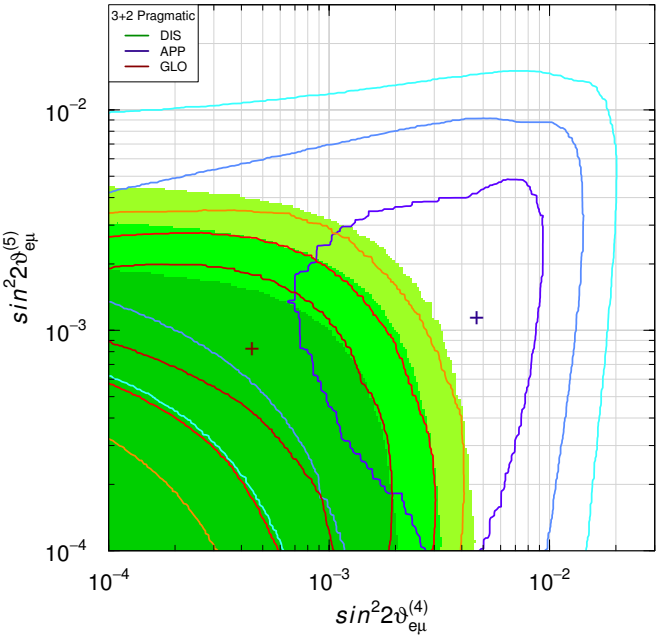

FIG. 8. Allowed regions in the $\sin^2 2\vartheta^{(4)}_{e\mu}$–$\sin^2 2\vartheta^{(5)}_{e\mu}$ plane obtained in the pragmatic 3+2 fit of short-baseline data corresponding to the 3+2-HIG fit of Ref. [44]. See the caption of Fig. 7. The green shadowed regions obtained from disappearance (DIS) data are the same of Fig. 7.

matic approach described above. The allowed regions in the $\sin^2 2\vartheta^{(4)}_{ee}$–$\sin^2 2\vartheta^{(4)}_{\mu\mu}$ plane in Fig. 4 obtained with the pragmatic 3+1 fit of short-baseline data show that the appearance-disappearance tension is acceptable. A comparison with Fig. 2 shows that the strips allowed by the analysis of short-baseline appearance (APP) data have moved towards smaller values of $\sin^2 2\vartheta^{(4)}_{ee}$ and $\sin^2 2\vartheta^{(4)}_{\mu\mu}$, which are in agreement with the analysis of disappearance data. The same behavior can be observed by confronting the two panels in Fig. 3, where one can see that in the pragmatic approach the intervals of $\sin^2 2\vartheta^{(4)}_{e\mu}$ allowed by the appearance and disappearance data overlap at about 1σ.

Let us now consider the 3+2 mixing scheme. Figures 5 and 6 show the marginal $\Delta\chi^2$ as a function of $\sin^2 2\vartheta^{(4)}_{e\mu}$ and $\sin^2 2\vartheta^{(5)}_{e\mu}$, respectively. They are different because the ordering $\Delta m^2_{41} \leq \Delta m^2_{51}$ breaks the degeneracy between the mixing of ν_4 and ν_5. Thanks to the relation (9), these figures are sufficient to visualize the appearance-disappearance tension.

The upper panel in Fig. 5 shows that in the total 3+2 fit there is no overlap of the intervals of $\sin^2 2\vartheta^{(4)}_{e\mu}$ allowed by the appearance and disappearance data at more than 2σ, which corresponds to an appearance-disappearance tension which is worse than that in the total 3+1 fit illustrated in the upper panel of Fig. 3 (see the discussion in Ref.[43]). On the other hand, the upper panel in Fig. 6 shows that the data do not constrain much the value of $\sin^2 2\vartheta^{(5)}_{e\mu}$ and the corresponding marginal $\Delta\chi^2$'s do not show an appearance-disappearance tension. However, it is clear that the manifestation of an appearance-disappearance tension in one of the oscillation amplitudes is enough.

The secondary local minimum at $\sin^2 2\vartheta^{(4)}_{e\mu} \approx 1.2 \times 10^{-3}$ of the appearance marginal $\Delta\chi^2$ in the upper panel in Fig. 5 is due to the possibility to fit the appearance data with $\sin^2 2\vartheta^{(4)}_{e\mu} \approx \sin^2 2\vartheta^{(5)}_{e\mu} \approx 1 - 2 \times 10^{-3}$ (with $\Delta m^2_{41} \approx 2\,\mathrm{eV}^2$ and $\Delta m^2_{51} \approx 4\,\mathrm{eV}^2$). This can be seen from the correlated allowed regions in the $\sin^2 2\vartheta^{(4)}_{e\mu}$–$\sin^2 2\vartheta^{(5)}_{e\mu}$ plane shown in Fig. 7 in which the 2σ region allowed by appearance data has a bulge for $\sin^2 2\vartheta^{(4)}_{e\mu} \approx \sin^2 2\vartheta^{(5)}_{e\mu} \approx 1 - 2 \times 10^{-3}$ (this type of figure has been already presented in Ref. [38]; similar figures for definite values of Δm^2_{41} and Δm^2_{51} have been presented in Ref. [26]). From this figure one can have another view of the appearance-disappearance tension, which is clearly dominated by $\sin^2 2\vartheta^{(4)}_{e\mu}$.

The lower panels of Figs. 5 and 6 and Fig. 8 illustrate the appearance-disappearance tension in the pragmatic 3+2 fit. One can clearly see that, as in the 3+1 case, it is much milder than that obtained in the total fit, indicating an acceptable fit of the data. The secondary local minimum at $\sin^2 2\vartheta^{(4)}_{e\mu} \approx 1.2 \times 10^{-3}$ of the appearance marginal $\Delta\chi^2$ in the lower panel in Fig. 5 is due to the same reasons as that in the upper panel explained above and corresponds to the swelling towards $\sin^2 2\vartheta^{(4)}_{e\mu} \approx \sin^2 2\vartheta^{(5)}_{e\mu} \approx 1 - 2 \times 10^{-3}$ of the 1σ region allowed by appearance data in Fig. 8.

In conclusion, in this paper we have derived the relation (9) (and its approximation (10)) between the amplitudes of short-baseline appearance and disappearance oscillations in $3+N_s$ neutrino mixing schemes. This relation is the origin of the appearance-disappearance tension that is found from the analysis of the existing data in any $3+N_s$ neutrino mixing scheme. We have illustrated the power of the relation (9) to reveal the appearance-disappearance tension in the cases of 3+1 and 3+2 mixing using the results of the fits of short-baseline neutrino oscillation data presented in Ref. [44].

ACKNOWLEDGMENTS

This work was partially supported by the research grant *Theoretical Astroparticle Physics* number 2012CPPYP7 under the program PRIN 2012 funded by the Ministero dell'Istruzione, Università e della Ricerca (MIUR). E. Z. thanks the support of funding grants 2013/02518-7 and 2014/23980-3, São Paulo Research Foundation (FAPESP).

[1] G. Bellini, L. Ludhova, G. Ranucci, and F. Villante, Adv.High Energy Phys. **2014**, 191960 (2014), arXiv:1310.7858.
[2] Y. Wang and Z. zhong Xing, arXiv:1504.06155.
[3] G. Mention *et al.*, Phys. Rev. **D83**, 073006 (2011), arXiv:1101.2755.
[4] T. A. Mueller *et al.*, Phys. Rev. **C83**, 054615 (2011), arXiv:1101.2663.
[5] P. Huber, Phys. Rev. **C84**, 024617 (2011), arXiv:1106.0687.
[6] SAGE, J. N. Abdurashitov *et al.*, Phys. Rev. **C73**, 045805 (2006), nucl-ex/0512041.
[7] M. Laveder, Nucl. Phys. Proc. Suppl. **168**, 344 (2007).
[8] C. Giunti and M. Laveder, Mod. Phys. Lett. **A22**, 2499 (2007), hep-ph/0610352.
[9] C. Giunti and M. Laveder, Phys. Rev. **C83**, 065504 (2011), arXiv:1006.3244.
[10] C. Giunti, M. Laveder, Y. Li, Q. Liu, and H. Long, Phys. Rev. **D86**, 113014 (2012), arXiv:1210.5715.
[11] F. Kaether, W. Hampel, G. Heusser, J. Kiko, and T. Kirsten, Phys. Lett. **B685**, 47 (2010), arXiv:1001.2731.
[12] SAGE, J. N. Abdurashitov *et al.*, Phys. Rev. **C80**, 015807 (2009), arXiv:0901.2200.
[13] LSND, C. Athanassopoulos *et al.*, Phys. Rev. Lett. **75**, 2650 (1995), nucl-ex/9504002.
[14] LSND, A. Aguilar *et al.*, Phys. Rev. **D64**, 112007 (2001), hep-ex/0104049.
[15] B. Pontecorvo, Sov. Phys. JETP **26**, 984 (1968).
[16] M. Sorel, J. Conrad, and M. Shaevitz, Phys. Rev. **D70**, 073004 (2004), hep-ph/0305255.
[17] G. Karagiorgi *et al.*, Phys. Rev. **D75**, 013011 (2007), hep-ph/0609177.
[18] M. Maltoni and T. Schwetz, Phys. Rev. **D76**, 093005 (2007), arXiv:0705.0107.
[19] G. Karagiorgi, Z. Djurcic, J. Conrad, M. H. Shaevitz, and M. Sorel, Phys. Rev. **D80**, 073001 (2009), arXiv:0906.1997.
[20] A. Donini, P. Hernandez, J. Lopez-Pavon, M. Maltoni, and T. Schwetz, JHEP **07**, 161 (2012), arXiv:1205.5230.
[21] A. E. Nelson, Phys. Rev. **D84**, 053001 (2011), arXiv:1010.3970.
[22] J. Fan and P. Langacker, JHEP **04**, 083 (2012), arXiv:1201.6662.
[23] E. Kuflik, S. D. McDermott, and K. M. Zurek, Phys. Rev. **D86**, 033015 (2012), arXiv:1205.1791.
[24] J. Huang and A. E. Nelson, Phys.Rev. **D88**, 033016 (2013), arXiv:1306.6079.
[25] J. Kopp, M. Maltoni, and T. Schwetz, Phys. Rev. Lett. **107**, 091801 (2011), arXiv:1103.4570.
[26] J. Kopp, P. A. N. Machado, M. Maltoni, and T. Schwetz, JHEP **1305**, 050 (2013), arXiv:1303.3011.
[27] N. Okada and O. Yasuda, Int. J. Mod. Phys. **A12**, 3669 (1997), hep-ph/9606411.
[28] S. M. Bilenky, C. Giunti, and W. Grimus, Eur. Phys. J. **C1**, 247 (1998), hep-ph/9607372.
[29] S. M. Bilenky, C. Giunti, and W. Grimus, Prog. Part. Nucl. Phys. **43**, 1 (1999), hep-ph/9812360.
[30] S. M. Bilenky, C. Giunti, W. Grimus, and T. Schwetz, Phys. Rev. **D60**, 073007 (1999), hep-ph/9903454.
[31] C. Giunti and M. Laveder, JHEP **02**, 001 (2001), hep-ph/0010009.
[32] O. Peres and A. Smirnov, Nucl.Phys. **B599**, 3 (2001), hep-ph/0011054.
[33] W. Grimus and T. Schwetz, Eur. Phys. J. **C20**, 1 (2001), hep-ph/0102252.
[34] M. Maltoni, T. Schwetz, M. A. Tortola, and J. W. F. Valle, Nucl. Phys. **B643**, 321 (2002), hep-ph/0207157.
[35] M. Maltoni, T. Schwetz, M. Tortola, and J. Valle, New J. Phys. **6**, 122 (2004), hep-ph/0405172.
[36] M. C. Gonzalez-Garcia and M. Maltoni, Phys. Rept. **460**, 1 (2008), arXiv:0704.1800.
[37] E. Akhmedov and T. Schwetz, JHEP **10**, 115 (2010), arXiv:1007.4171.
[38] C. Giunti and M. Laveder, Phys.Rev. **D84**, 073008 (2011), arXiv:1107.1452.
[39] C. Giunti and M. Laveder, Phys.Rev. **D84**, 093006 (2011), arXiv:1109.4033.
[40] C. Giunti and M. Laveder, Phys. Lett. **B706**, 200 (2011), arXiv:1111.1069.
[41] J. Conrad, C. Ignarra, G. Karagiorgi, M. Shaevitz, and J. Spitz, Adv.High Energy Phys. **2013**, 163897 (2013), arXiv:1207.4765.
[42] M. Archidiacono, N. Fornengo, C. Giunti, and A. Melchiorri, Phys. Rev. **D86**, 065028 (2012), arXiv:1207.6515.
[43] M. Archidiacono, N. Fornengo, C. Giunti, S. Hannestad, and A. Melchiorri, Phys.Rev. **D87**, 125034 (2013), arXiv:1302.6720.
[44] C. Giunti, M. Laveder, Y. Li, and H. Long, Phys.Rev. **D88**, 073008 (2013), arXiv:1308.5288.
[45] S. Bilenky, arXiv:1208.2497.
[46] S. Bilenky, Phys. Part. Nucl. Lett. **12**, 453 (2015), arXiv:1502.06158.
[47] MiniBooNE, A. A. Aguilar-Arevalo *et al.*, Phys. Rev. Lett. **102**, 101802 (2009), arXiv:0812.2243.
[48] MiniBooNE, A. Aguilar-Arevalo *et al.*, Phys.Rev.Lett. **110**, 161801 (2013), arXiv:1303.2588.
[49] MicroBooNE, H. Chen *et al.*, (2007), FERMILAB-PROPOSAL-0974.
[50] ArgoNeuT, MicroBooNE, A. M. Szelc, AIP Conf. Proc. **1666**, 180001 (2015).